Canadian Geotechnical Journal

Discussion of "Determination of the critical state of a silty sand iron tailings in triaxial extension tests using photographic correction"

Lin Li and Zhenwang Chen

College of Civil Engineering, Nanjing Forestry University, No.159 Longpan Road, Nanjing 210037, Jiangsu, China

Corresponding author: **Lin Li** (email: lli2018@njfu.edu.cn)

Accurate volume/deformation measurement on triaxial specimen using image-based method is challenging. The major difficulty lies on the fact that the specimen is located in a triaxial chamber filled with confining fluid and subjected to significant distortion due to refraction. Becker et al. (2022) presented a method to measure the deformation of soil specimens during drained triaxial tests. Specifically, this method utilized a single, external smartphone camera to capture images of a specimen within a triaxial chamber filled with water. Several issues regarding the photographic correction, not explicitly explained in Becker et al. (2022), are discussed.

Two photographs of a cylindrical soil specimen with a diameter-to-height ratio of 1:2 in a triaxial cell are shown in Figs. 1*a* and 1*b*. The left (i.e., Fig. 1*a*) is captured using an external camera at a distance of approximately 80 cm away from the specimen and the right is captured using the same camera at a much shorter distance, approximately 15 cm. In Fig. 1*a*, the specimen appears to be cylindrical and the distortion along the axial direction is not significant. However, significant distortion along the radial direction does exist and results in a reduction in specimen height/diameter ratio on the photograph. At a short camera-to-specimen distance, as shown in Fig. 1*b*, significant distortion along the radial direction can be easily identified. The distortion due to refraction is not uniform and highly dependent on both endogenous and exogenous causes. The endogenous cause is the shape of the triaxial cell wall and confining fluid, the exogenous cause is the incident angle of the optical ray from camera to specimen, which is dependent on the relative position between camera and specimen. Proper handling of the refraction is considered as the key to an accurate volume/deformation measurement on triaxial specimens. In Becker et al. (2022), the photographic correction was made separately for the distortion in axial and radial directions.

Photographic correction along axial direction

In Becker et al. (2022), the relative positions of the camera, triaxial cell wall, and specimen are given as shown in Fig. 2*a*. The photographic correction along the axial direction is schematically addressed as follows: an optical ray travels from the camera focus O, reaches the cell wall at E, the inner wall at F, and then stopped at A on specimen surface. The five angles (i.e., θ_0–θ_4) and the coordinates of E and F in Fig. 2*a* are the unknowns. The Snell's law can be applied for the refraction at the air–cell and cell–water interfaces (i.e., eq. 1). According to trigonometry, eq. 2 should hold. Together with $\theta_0 = \theta_1$ and $\theta_2 = \theta_3$, those five angles can then be calculated as shown in Fig. 2*a*. The θ_5 can also be calculated with the AD and OD. It should be noted that the virtual point of A is located at A' instead of B according to Butler et al. (2002). This is the reason why when we look down into a pool of water from above, the pool looks less deep than it really is. In addition, the virtual specimen is not perfectly cylindrical on the photograph. Instead, the edge AD turns into a curved line $A'D'$ as shown in Fig. 2*a*, which is confirmed by Fig. 1*b*. It should be noted that a longer camera-to-specimen distance is helpful to reduce this distortion along the axial direction.

$$(1)\qquad n_a \cdot \theta_{0/1} = n_c \cdot \theta_{2/3},\ n_c \cdot \theta_{2/3} = n_w \cdot \theta_4$$

$$(2)\qquad \tan\theta_{0/1} \cdot OH + \tan\theta_{2/3} \cdot GH + \tan\theta_4 \cdot GD = AD$$

where, n_a, n_c, and n_w are the refractive indices of air, cell wall, and water.

Becker et al. (2022) addressed that the ratio between the apparent and real heights, $H_{app}/H_{real} = 1.0018$. Actually, this ratio should be equal to 1 since the height of the virtual specimen is the same as that of the real specimen according to Fig. 2*a*. Using the image plane where points E, H are located as an example, the scale, which is the ratio between the apparent (i.e., real height) and height of the specimen on the photo (i.e., $H_{1stphoto}$), $= AD/EH = 1.029$. At an axial strain of 15%, the height of the specimen increased from 5.00 to 5.75 cm. Similarly, new θ_0, θ_2, θ_4 are calculated to be 3.298°, 2.213°, 2.476°. The height of the specimen on the photo (i.e., H_{photo}, equivalent to the updated EH) is 5.589 cm. With this H_{photo}, and the scale, the specimen height is calculated to be 5.75004 cm, which confirms that a scale can be utilized to measure speci-

Fig. 1. Photograph distortion due to refraction.

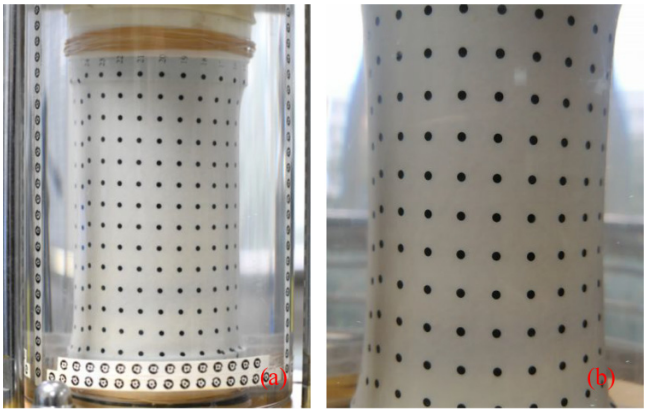

men height along the axial direction at high accuracy even at a strain level up to 15%, and the ratio between the apparent and real heights, H_{app}/H_{real} presented in Becker et al. (2022) is not required.

Photographic correction along radial direction

The photographic correction along the radial direction can be performed using the two-dimensional refraction correction model proposed by Macari et al. (1997) for triaxial specimens along the radial direction. To facilitate the calculation, a two-dimensional coordinate system is built. The center of the specimen O_0, as shown in Fig. 2*b*, is set as the origin of this coordinate system, *x*-axis is set to be horizontal and pass through the focus of the camera (i.e., *O*), *y*-axis is set to be vertical. An optical ray travels from the camera focus *O*, reaches the cell wall at *E*, the inner wall at *F*, and then stopped at *A*

Fig. 2. Two-dimensional models for refraction correction.

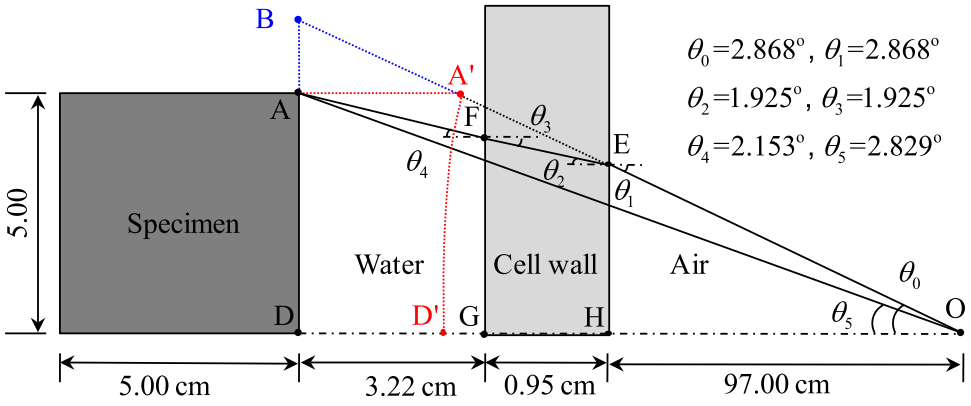

(a) Axial direction

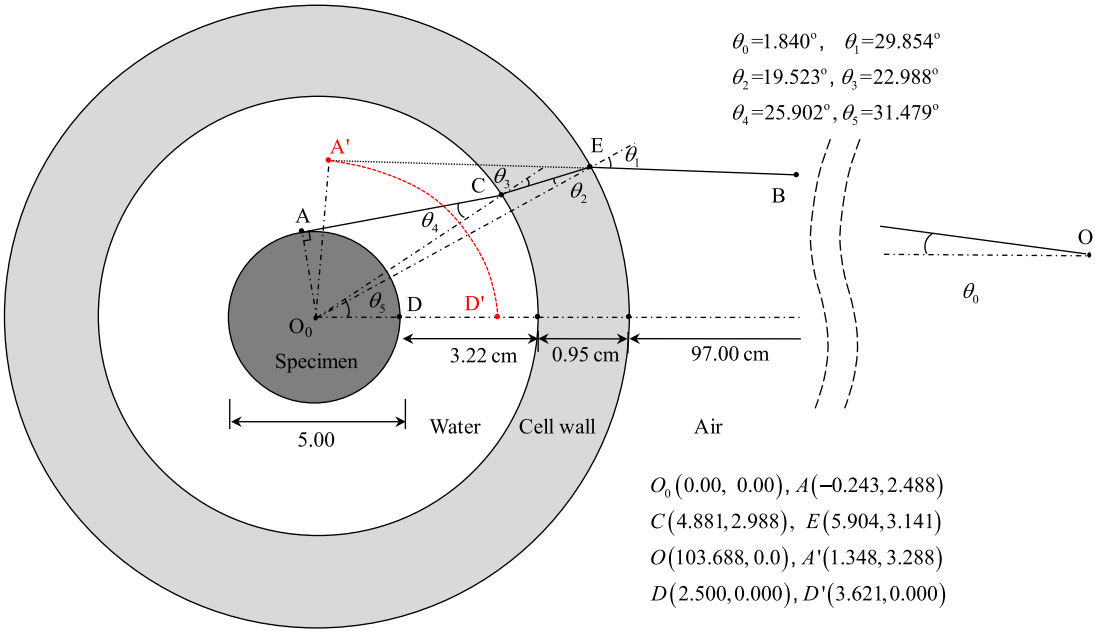

(b) Radial direction

on specimen surface. Similarly, the five angles (i.e., θ_0–θ_4) and coordinate of points *A, C, E* in Fig. 2*b* are the unknowns. For the triangle O_0AC, $\sin\theta_4$ is equal to O_0A/O_0C since *CA* is tangential to the specimen surface. As a result, θ_4 can be determined based on O_0A (i.e., the radius of the specimen) and O_0C (i.e., the radius of the cell inner surface). We can give an initial guess of $\angle CO_0D = \theta_5$, and the coordinates of point *C* can be calculated. By applying Snell's law (Zhang et al. 2015) at the cell–water interface, θ_3 can be solved. With point *C*, θ_3 and θ_5, the coordinates of point *E* and θ_2 can then be obtained. By applying Snell's law at the cell–air interface, θ_1 can then be calculated. With θ_1, $\angle EO_0O$, and point *E*, the optical ray *EB* can be built. According to Fig. 2*b*, this optical ray should exactly pass through the focus of camera, *O*. With this condition, θ_5 (i.e., the initial guess) can be back-calculated and the rest unknowns are updated in Fig. 2*b*. According to the model proposed by Macari et al. (1997), the ratio between the apparent and real diameters, D_{app}/D_{real} is determined to be 1.4213 instead of 1.3301 as specified in Becker et al. (2022).

Virtual point determination

As shown in Fig. 1, two photographs are subjected to significant distortions due to refraction and the specimen on the photographs is virtual. A variation in camera orientation will bring a different virtual specimen on the photograph (e.g., Fig. 1*b* and 1*c*). In other words, the virtual specimen is not unique. According to Butler et al. (2002), the length of the virtual optical ray is equal to the length of the actual optical ray divided by the refractive index of water. With the help of this, the location of the virtual specimen can be calculated. Figure 2 schematically plots the position of the virtual specimen, which is consistent with that shown in Figs. 1*b* and 2*c*.

In summary, the use of ratios/scales for photographic correction is convenient for a quick specimen volume measurement. However, errors will inevitably be generated due to the way in handling refraction and these errors are highly dependent on the match between the system set-up and refraction correction model as typically shown in Fig. 2. Besides, in real measurements, the distortions are in three-dimensional (3D) and the suitability of the two-dimensional refraction correction models in Fig. 2 is questionable. Aiming at a high-accuracy volume/deformation measurement on triaxial specimens, the multi-media photogrammetry with help of a ray tracing technique (e.g., Zhang et al. 2015; Li et al. 2016,2021) is recommended since it can rigorously handle 3D optical ray refraction.

Article information

History dates

Received: 1 December 2022
Accepted: 9 January 2023
Accepted manuscript online: 17 May 2023
Version of record online: 17 May 2023

Notes

Article appears in the Canadian Geotechnical Journal, 60: 504–520. doi: 10.1139/cgj-2021-0637.

Copyright

Data availability

All data are already included in the Discussion.

Author information

Author ORCIDs

Lin Li https://orcid.org/0000-0002-0950-8412

Author contributions

Conceptualization: LL
Data curation: LL
Formal analysis: LL
Methodology: LL
Validation: ZC

Competing interests

No conflict of interests.

Funding information

No funding for this submission.

References

Becker, L.D.B, Fabre, J.S., and Barbosa, M.C. 2022. Determination of the critical state of a silty sand iron tailings in triaxial extension tests using photographic correction. Canadian Geotechnical Journal. doi:10.1139/cgj-2021-0637.

Butler, J., Lane, S., Chandler, J., and Porfiri, E. 2002. Through-water close range digital photogrammetry in flume and field environments. The Photogrammetric Record, **17**(99): 419–439. doi:10.1111/0031-868x.00196.

Li, L., Zhang, X., Chen, G., and Lytton, R. 2016. Measuring unsaturated soil deformations during triaxial testing using a photogrammetry-based method. Canadian Geotechnical Journal, **53**(3): 472–489. doi:10.1139/cgj-2015-0038.

Li, L., Li, P., Cai, Y., and Lu, Y. 2021. Visualization of non-uniform soil deformation during triaxial testing. Acta Geotechnica, **16**: 3439–3454. doi:10.1007/s11440-021-01310-w.

Macari, E.J., Parken, J., and Costes, N.C. 1997. Measurement of volume changes in triaxial tests using digital imaging techniques. ASTM Geotechnical Testing Journal, **20**(1): 103–109.

Zhang, X., Li, L., Chen, G., and Lytton, R.L. 2015. A photogrammetry-based method to measure total and local volume changes of unsaturated soils during triaxial testing. Acta Geotechnica, **10**(1): 55–82. doi:10.1007/s11440-014-0346-8.